

cedure with plateaus ensured that we always had a quasi-steady state (thermodynamic equilibrium) in the melt.

Figures 5(a) and (b) are background subtracted images taken at the point of appearance of the first solid at the two end walls, respectively. First, solid appeared at the lower left end wall of the test cell, while a small amount of solid also appeared on the middle portion of the left end wall of the cavity. The temperature at which the solid appeared is designated as the first critical temperature $T_{c1} = 19.0$ °C. Upon further cooling at a very slow cooling rate, at a second critical temperature $T_{c2} = 18.9$ °C, solid started appearing at the right end wall toward the base of the test cell (picture not shown). Figure 5(b) is an image taken after 12.78 hours of cooling, which shows a small amount of solid at the right end wall and evidences the disappearance of a crystal grown at one-third height of the left end wall in Figure 5(a). Note that the coolant flow in the thermodes was from top to bottom, which means that with a room temperature of 25 °C and inherent insulation deficiencies, the temperature at the bottom of the thermode might have been slightly higher at the bottom of the melt.

From the phase diagram,^[1] the liquidus temperature of 18.9 °C or 19.0 °C correlates to a concentration of 23.0 ± 1 wt pct In (~ 15.3 at. pct), which must exist at the bottom of the melt, assuming the phase diagram is accurate. Those values are different from the eutectic composition of 21.4 wt pct In (14.2 at. pct) of the mixture. Assuming a thermodynamically closed system with vertical stratification and eutectic composition at midheight of the melt layer, a gravitational segregation of 3.2 ± 1 wt pct In (~ 2.2 at. pct) is estimated. This is in contrast to the negligible gravitational segregation obtained with activity coefficients from conventional theory.^[7] The observed segregation is much higher than the theoretical value.

As our visualization is hampered by the required lead frame around the melt, some information at the end walls is lost. Thus, the crystals of indium may start to grow at even slightly higher temperatures of the isothermal melt. The observed gravitational segregation may therefore be even more substantial than calculated. Such a significant gravitational segregation may be the cause of manufacturing problems with many industrially important alloys.^[8]

Support by the National Science Foundation (NSF) under Grant Nos. CTS-8906846 and CTS-9114775 and the National Aeronautics and Space Administration (NASA) under Grant No. NCC3-210 is greatly appreciated. The authors thank A. Grötzbach for his contributions to this experiment.

REFERENCES

1. C.E.T. White and H. Okamoto: *Phase Diagrams of Indium Alloys and Their Engineering Applications*, Monograph Series on Alloy Phase Diagrams, 1st ed., ASM INTERNATIONAL, Materials Park, OH, 1992, p. 2.
2. P.G. Barber, R.K. Crouch, A.L. Fripp, W.J. Debnam, R.F. Berry, and R. Simchick: *J. Cryst. Growth*, 1986, vol. 74, pp. 228-30.
3. K. Kakimoto, M. Eguchi, H. Watanabe, and T. Hibiya: *J. Cryst. Growth*, 1988, vol. 88, pp. 365-70.
4. T.A. Campbell and J.N. Koster: *J. Cryst. Growth*, 1994, vol. 140, pp. 414-25.

5. R.E. Pool and J.N. Koster: *Int. J. Heat Mass Transfer*, 1994, vol. 37, pp. 2583-87.
6. R. Derebail and J.N. Koster: *Metall. Mater. Trans. B*, 1996, unpublished research.
7. R.T. DeHoff: *Thermodynamics in Materials Science*, McGraw-Hill, Inc., New York, NY, 1993, pp. 442-44.
8. J. Schilz and V.N. Romanenko: *J. Mater. Sci.: Mater. Electronics*, 1995, vol. 6, pp. 265-79.

Prediction of Dendrite Arm Spacing for Low Alloy Steel Casting Processes

M. EL-BEALY and B.G. THOMAS

Simple mathematical expressions to predict the primary dendrite arm spacing (PDAS) and secondary dendrite arm spacing (SDAS) suitable for steel casting processes are presented. The equations of the PDAS and SDAS were based on previously published experimental data for low alloy steels. Good agreement was obtained between previous measurements of dendrite arm spacing (DAS) and model predications in the range of cooling rate occurring in steel casting processes. The results indicated that the cooling rate and carbon content basically govern the calculation of PDAS, especially for low carbon steel. However, the carbon content governs the selection of mathematical expression to predict SDAS for low alloy steels.

Dendritic growth is the most common crystallization mechanism in industrial steels. Many descriptive studies characterize the microstructure of metal alloy solidification in terms of the dendrite morphology. The dendrite morphology defines a dendrite as composed of primary, secondary, and higher order arms.^[1] The fineness of the dendritic structure affects microsegregation and inclusion formation, which leads to a deterioration in mechanical properties.^[2]

Most of the published work concerning dendrite arm spacing (DAS) has involved the postmortem examination of solidified steel ingots in which the solidification conditions have been only partially controlled.^[3-6] It is generally agreed that both thermal conditions and alloy content affect the structure of cast steel alloys. The measured parameter has been the local cooling rate, or the local solidification time, whereas the local dendrite tip velocity and temperature gradient were unknown. Nevertheless, these experiments have contributed greatly to our understanding of dendrite morphology. A few attempts have been made to control solidification more precisely by establishing steady-state columnar dendrite growth conditions with controlled growth velocities and the known temperature gradient.^[7,8,9] Increasing the cooling rate is known to reduce both the primary dendrite arm spacing (PDAS) and the secondary dendrite arm spacing (SDAS).^[11-9] Also, it has been shown

M. EL-BEALY, Research Associate, and B.G. THOMAS, Associate Professor, are with the Department of Mechanical and Industrial Engineering, University of Illinois at Urbana-Champaign, Urbana, IL 61801.

Manuscript submitted December 19, 1995.

Table I. Expression Developed to Estimate the PDAS

Equation	Equation Parameters	Equation Number
$\lambda_1 = K(C_R)^m(C_0)^n$ (μm)	$K = 278.748$ $m = -0.206277638$ $0 \leq C_0 \leq 0.15$ $n = -0.316225 + 2.0325C_0$ (wt pct C) $0.15 \leq C_0 \leq 1.0$ $n = -0.0189 - 0.491666C_0$ (wt pct C)	Eq. [1]

Table II. Expressions Developed to Estimate the SDAS

Equation	Equation Parameters	Equation Number
$0 \leq C_0 \leq 0.53$		Eq. [2]
$\lambda_2 = A_1(C_R)^{-n}$ (μm)	$A_1 = 148$ $n = 0.38$	
$0.53 \leq C_0 \leq 1.5$		Eq. [3]
$\lambda_2 = A_2(t_f)^d$ (μm)	$A_2 = 21.52764 - 9.40C_0$ (wt pct C) $d = 0.4 + 0.08C_0$ (wt pct C)	

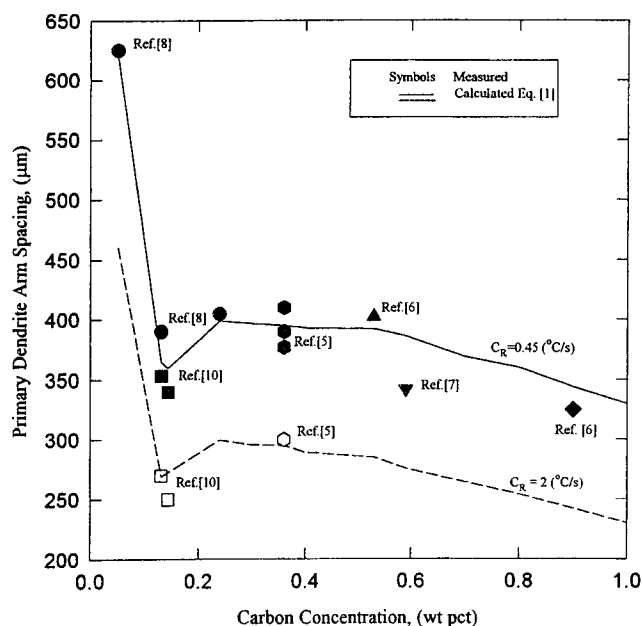


Fig. 1—Comparison between measured PDAS according to Refs. 5 through 8 and 10 and calculated PDAS by using Eq. [1] as a function of the carbon concentration with two different cooling rates.

that secondary arm spacing increases with time spent in the liquid-solid region.

Many empirical expressions have been employed to correlate the PDAS and SDAS with growth rate, temperature gradient, cooling rate, and local solidification time.^[1-10] However, the comparative advantages of the various expressions with respect to the accuracy with different types of steels remain unclear. Thus, the aim of the present study is to develop simple expressions to predict DAS as a function of carbon content and thermal conditions of low alloy steels.

In the present study, the primary arm spacing λ_1 was calculated as a function of cooling rate C_R ($^{\circ}\text{C/s}$) and nominal steel carbon content C_0 (wt pct) from the following equation:

$$\lambda_1 = K(C_R)^m(C_0)^n \quad (\mu\text{m}) \quad [1]$$

Equation [1] was formulated by fitting the previous experimental data^[5-8,10] for different types of steel to the preceding empirical equation. The values of the constant K and exponents m and n in Eq. [1] are summarized in Table I.

As stated earlier,^[3,7] both experimental and theoretical analyses have linked SDAS empirically to other solidification parameters. The SDAS profile was evaluated as a function of cooling rate^[1,3] and solidification time.^[7] The expressions were chosen to cover the known SDAS dependence on heat-transfer parameters and carbon content.

The secondary arm spacing λ_2 was calculated as a function of cooling rate for steels containing less than 0.53 wt pct C and the following equation was employed:

$$\lambda_2 = A_1(C_R)^{-n} \quad (\mu\text{m}) \quad [2]$$

In the case of steels containing more than 0.53 wt pct C, the SDAS was computed as a function of local solidification time t_f from the following equation:

$$\lambda_2 = A_2(t_f)^d \quad (\mu\text{m}) \quad [3]$$

where

$$t_f = \frac{T_{\text{liq}} - T_{\text{sol}}}{C_R} \quad (\text{s}) \quad [4]$$

where T_{liq} and T_{sol} are liquidus and solidus temperatures. The parameters A_1 , n , A_2 , and d employed in Eqs. [2] and [3] were calculated by fitting the experimental data in References [3] and [7] to these equations. The values of these parameters are summarized in Table II.

The mathematical expressions for DAS predicted by the present empirical model are based on the experimental^[3-8,10] and theoretical^[3,7] data in the literature for different types of low steels. The experimental DAS were measured using the standard line method^[7,9] with quantitative optical microscopy. The error in this method normally is within 5 pct.^[2]

Figure 1 compares the calculated and measured PDAS. The predicted curve fits very well with the experimental points. Some deviation is observed at the higher carbon content. This may be due to the effect of macro-microsegregation in the high carbon steel.^[12] Figure 1 illustrates also that the PDAS decreases with increases in cooling rate for all types of steels.

Figure 1 reveals that the variation in the PDAS as a function of cooling rate depends significantly on the carbon content, especially in steels with low carbon contents. This is probably because different solidification modes control the evolution of structure.^[11] These solidification modes may be classified into four ranges, as shown in Figure 2.

The PDAS decreases steeply with increasing carbon concentration from 0.05 to its minimum value at 0.15 wt pct C. In the first range ($0 \rightarrow 0.09$ wt pct C), when the melt cools down slightly below the liquidus temperature, the PDAS begins to nucleate and grows as delta phase, δ , until the end of solidification.

However, in the second range ($0.09 \rightarrow 0.15$ wt pct C),

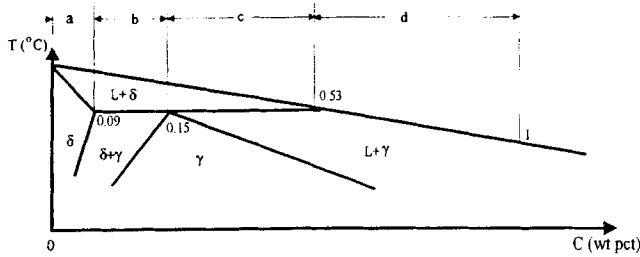


Fig. 2—Schematic representation of Fe-C phase diagram and its different solidification modes: (a) first mode, (b) second mode, (c) third mode, and (d) fourth mode.

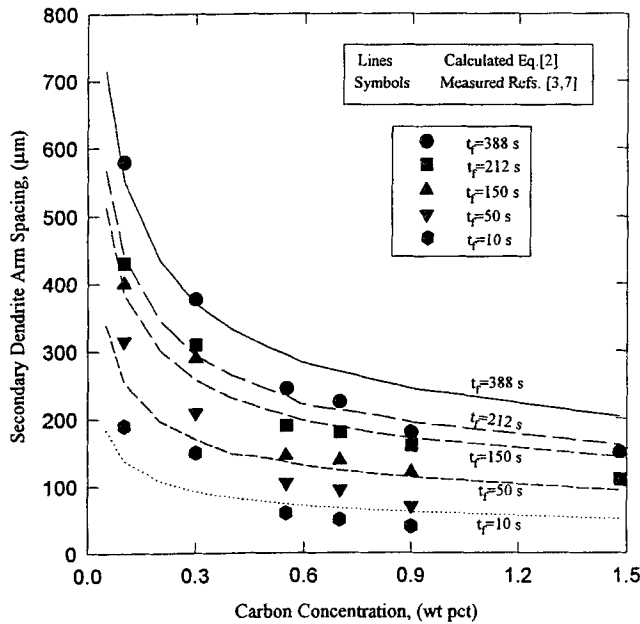


Fig. 3—Comparison between measured SDAS according to Refs. 3 and 7 and calculated PDAS by using Eqs. [2] and [4] as a function of the carbon concentration under different solidification times.

the PDAS nucleates and grows as primary delta phase, δ , only until the peritectic temperature. At the peritectic temperature, the solid austenite forms around the periphery of the δ phase, a fact which has led to the name "peritectic reaction $L + \delta \rightarrow \gamma$."^[11,12] This reaction is relatively rapid and is governed by diffusion through the secondary and liquid phases which may affect the growth of PDAS.^[11]

The PDAS increases again with an increase in carbon content until 0.24 wt pct C. This variation is due to the change in the peritectic solidification mode. The PDAS nucleates and grows as delta phase, $L \rightarrow \delta$, until the peritectic temperature. Then, an austenite layer solidifies $L \rightarrow \gamma$ and covers the primary phase until the end of solidification. At the same time, the primary delta transforms to secondary austenite. This mode may govern the evolution of DAS within the third range (0.15 \rightarrow 0.53 wt pct C).^[13] From 0.24 to 0.53 wt pct C, the PDAS decreases slightly because there is no change in the solidification mode.

In the fourth range (0.53 \rightarrow 1 wt pct C), the PDAS decreases gradually because the solid nucleates from the melt and grows as austenite phase until the end of solidification.

Figures 3 and 4 show the comparison between the experimental data^[3,7] of SDAS and the model predictions for different carbon contents. Figure 3 shows the SDAS cal-

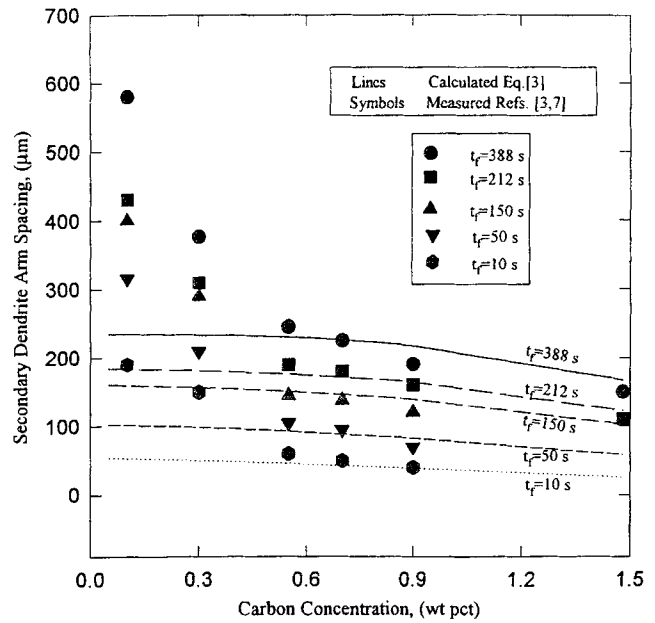


Fig. 4—Comparison between measured SDAS according to Refs. 3 and 7 and calculated PDAS by using Eq. [3] as a function of the carbon concentration under different solidification times.

culated by Eqs. [2] and [4], and Figure 4 illustrates the SDAS calculated by Eq. [3].

The results show that the SDAS calculated as a function of cooling rate (Eq. [2]) fits well only with measured results for steels containing from 0.1 to approximately 0.53 wt pct carbon, as shown in Figure 3. However, the SDAS calculated by Eq. [3] as a function of solidification time agrees well only with measured results for steels containing higher than 0.53 wt pct carbon, as shown in Figure 4. These results agree qualitatively and quantitatively well with the results by Suzuki *et al.*^[3] for low carbon steels and by Jacobi and Schwerdtfeger^[7] for high carbon steels. The figures also indicate that the SDAS decreases with increasing cooling rate or decreasing solidification time. Furthermore, the SDAS decreases with increasing carbon content, as seen in Figures 3 and 4.

Examination of the preceding DAS profiles suggests that a change in solidification mode from ferrite and austenite has a significant effect on the DAS. This is because DAS, particularly SDAS, is controlled by a coarsening process. In this process, the dendrite arms first grow at very small spacing near the tip of the dendrite. As solidification continues, the dendrite attempts to reduce its surface energy by reducing its surface area. Small arms preferentially go into solution, while larger arms grow at their expense. Thus, the average spacing between arms increases. The rate of this process appears to be limited by the rate of diffusion of solute in the liquid as the solute transfers between dissolving and growing arms.^[14] Previous work pointed out that the rate of diffusion of carbon in the open bcc lattice (δ ferrite) is faster than in the more closely packed fcc (γ austenite).^[14] This may explain the difference in the evolution mechanism of DAS of different carbon steels.

Figures 5(a) and (b) compare the PDAS and SDAS calculated from the present expressions with DAS computed using the available expressions in the literature given in Table III.^[3,7] As seen in Table III, most of the previous

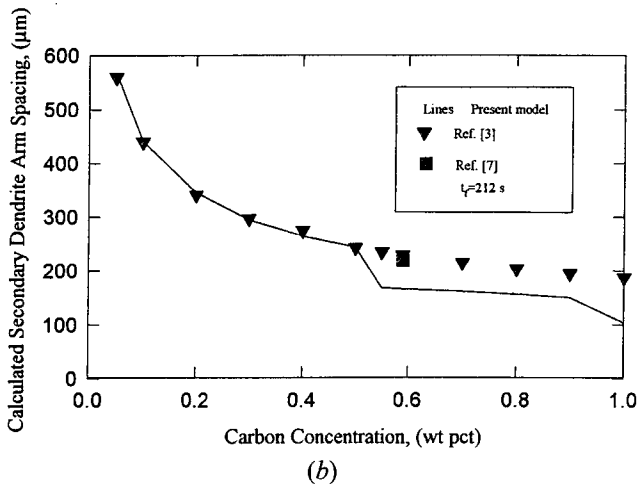
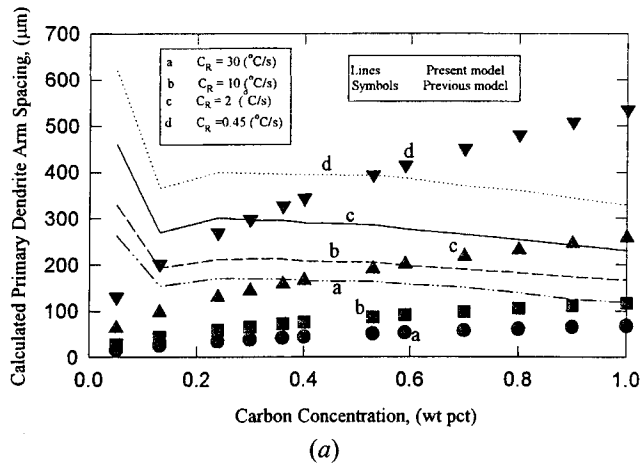


Fig. 5—Comparison between calculated DAS by using Eqs. [1] through [4] and calculated DAS by using data in Table III as function of the carbon concentration with different cooling rates: (a) PDAS and (b) SDAS.

Table III. Literature Expressions to Estimate the DAS^[3,7]

Equations	Steel Alloys
DAS^[7]	
$\lambda_1 = 35.6 \times t_f^{0.44} = 283 \times C_R^{-0.49}$	(μm) Fe-0.59 wt pct C
$\lambda_2 = 15.8 \times t_f^{0.44}$	(μm) Fe-0.59 wt pct C
SDAS^[3]	
$\lambda_2 = 148 \times C_R^{-0.38}$	(μm) Fe-0.1 to 0.9 wt pct C

equations accurately predict DAS for only one type of steel over a limited range of cooling rates. Even the formula of Suzuki *et al.*,^[3] which is valid over a large range of low alloy steels, loses accuracy for high carbon steels, as shown in Figure 5(b). The present equations appear to be accurate over a large range of low alloy steels.

The large DAS may increase the interdendritic areas and concentrations of solute elements in the interdendritic liquid.^[14] A coarse structure also tends to increase the microsegregation of solute and impurity elements and, consequently, the related cracking susceptibility of the steel.^[15] Also, the increase in the interdendritic areas and interdendritic concentrations of solute elements may help the inclusions to grow.^[14] This yields an increase in their size and volume fraction,^[2,15] which impairs the mechanical properties of cast steel to some degree. As a result, the

susceptibility of crack formation^[16,17,18] in cast steel and breakouts^[19] in continuously cast steel will increase.

Simple expressions have been developed to accurately predict the PDAS and SDAS during solidification of a wide range of low alloy steels. The model is based on the published experimental data.^[3-8,10]

The main results and conclusions from this work are the following.

1. The cooling rate and steel carbon content govern the calculation of PDAS.
2. The carbon content and cooling rate or solidification time control the calculation of SDAS.
3. The carbon content governs the selection of the mathematical expression to calculate SDAS.

Although the predications of the model are generally supported by the published experimental results, it is still necessary to refine the model and resolve some remaining problems by both experimental work and numerical modeling. Another important aspect of the future work is to modify and extend the model to high alloy steels (multiple-composition alloys), in particular, Fe-C-Cr and Fe-C-Cr-Ni alloy systems. The model will be incorporated into a heat flow model and fluid flow model to predict quantitatively the macroscopic and microscopic behaviors of continuous casting of steel, especially defect formation such as inclusions and crack formation during processing, which is strongly associated with the microstructure evolution.

This work was supported by continuous casting consortium LTV Steel, Armco Inc, Inland Steel Co., AK Steel, Allegheny Ludlum and BHP. The authors acknowledge their support.

REFERENCES

1. M.C. Flemings: *Solidification Processing*, McGraw-Hill Book Co., New York, NY, 1974, p. 148.
2. N.A. Shah and J.J. Moore: *Metall. Trans. B*, 1989, vol. 20B, pp. 893-910.
3. A. Suzuki, T. Suzuki, Y. Nagaoka, and Y. Lwata: *Nippon Kinzoku Gakkaishi*, 1968, vol. 32, pp. 1301-05.
4. A. Suzuki and Y. Nagaoka: *J. Jpn. Inst. Met.*, 1969, vol. 33, pp. 658-64.
5. I. Lare'n and H. Fredriksson: *Scand. J. Metall.*, 1972, vol. 1, pp. 59-68.
6. M. El-Bealy: University of Illinois at Urbana-Champaign, Urbana, IL, unpublished research, 1995.
7. H. Jacobi and K. Schwerdtfeger: *Metall. Trans. A*, 1976, vol. 7A, pp. 811-20.
8. Y. Ueshima, S. Mizoguchi, T. Matsumiya, and H. Kajjioka: *Metall. Trans. B*, 1986, vol. 17B, pp. 845-59.
9. K. Schwerdtfeger: *Arch. Eisenhuettenwes.*, 1970, vol. 41, pp. 923-37.
10. M. El-Bealy: *Scand. J. Metall.*, 1995, vol. 24, pp. 106-20.
11. H. Fredriksson and J. Stjerndahli: *Met. Sci.*, 1982, vol. 16, pp. 575-85.
12. Y.K. Chuang, D. Reinisch, and K. Schwerdtfeger: *Metall. Trans. A*, 1975, vol. 6A, pp. 235-45.
13. H. Fredriksson: *Solidification and Casting of Metals*, The Metals Society, London, 1977, p. 131.
14. J. Campbell: *Castings*, Butterworth-Heinemann Ltd., Oxford, 1991, pp. 9-268.
15. J.J. Moore and N.A. Shah: *CIM Annual Conf. Symp. on Continuous Casting of Steel*, Vancouver, BC, Canada, 1985, CIM, Montreal, PQ, Canada, 1985, pp. 5-32.

16. J.K. Brimacombe and K. Sorimachi: *Metall. Trans. B*, 1977, vol. 8B, pp. 489-505.
17. J.K. Brimacombe, F. Weinberg, and E.D. Hawbolt: *Metall. Trans. B*, 1979, vol. 10B, pp. 279-92.
18. H. Fredriksson: *Can. Metall. Q.*, 1991, vol. 30, pp. 235-44.
19. A. Grill, K. Sorimachi, and J.K. Brimacombe: *Metall. Trans. B*, 1976, vol. 7B, pp. 177-89.

Discussion of "Representation of Mixed Reactive Gases on Free Energy (Ellingham-Richardson) Diagrams"*

D.R. GASKELL

In a recent publication, Robino⁽¹⁾ considered the reduction of metal oxides by gaseous mixtures of atomic and molecular hydrogen. The following is offered as a thermodynamic analysis of reduction by hydrogen and the equilibria attained in hydrogen-water vapor mixtures.

The reducing power of an H₂-H₂O gas mixture is determined by the oxygen potential (partial pressure of oxygen) in the gas, which, in turn, is determined by the ratio of H₂ to H₂O in the gas. The system has two components ($C = 2$; hydrogen and oxygen), and if it is considered that three species ($N = 3$; H₂, O₂, and H₂O) occur in the system, then the number, R , of independent reaction equilibria in the system is given by $R = N - C = 1$, which is obviously



Consider an equimolar mixture of H₂ and H₂O equilibrated at 2000 K and a total pressure of 1 atm. At 2000 K,

$$\Delta G_{(1)}^\circ = -273,700 \text{ J and } K_{(1)} = 1.407 \times 10^7$$

Thus, with $p_{\text{H}_2} = p_{\text{H}_2\text{O}} = 0.5 \text{ atm}$, the equilibrium oxygen pressure, p_{O_2} , in the gas mixture is obtained from

$$K_{(1)} = 1.407 \times 10^7 = \frac{0.5^2}{0.5^2 p_{\text{O}_2}}$$

as $p_{\text{O}_2} = 7.11 \times 10^{-8} \text{ atm}$.

If it is considered that the equilibrated gas contains atomic hydrogen, then the two-component system contains four species and involves two *independent* reaction equilibria, which are most conveniently chosen as the equilibrium given by Eq. [1] and



At 2000 K,

$$\Delta G_{(2)}^\circ = -225,760 \text{ J and } K_{(2)} = 7.87 \times 10^5$$

These independent equilibria may not be combined to produce an equation which is considered to be the sole independent equilibrium.

Consider the equilibrium reached in the four-species

mixture when 1 mole of H₂ is mixed with 1 mole of H₂O at 2000 K and 1 atm pressure. In considering the equilibrium given by Eq. [1], the 1 mole of H₂O partially dissociates to produce x moles of O₂, $(1 + 2x)$ moles of H₂, and $(1 - 2x)$ moles of H₂O. Then, in considering the equilibrium given by Eq. [2], the $(1 + 2x)$ moles of H₂ partially dissociate to produce $2y$ moles of H and $(1 + 2x - y)$ moles of H₂. The system now contains a total number of moles, n_T , of $(2 + x + y)$, and the partial pressure, p_i , of each species, at a total pressure of 1 atm, is given by

$$p_i = \frac{n_i}{n_T}$$

Thus, for the equilibrium given by Eq. [1],

$$1.407 \times 10^7 = \frac{p_{\text{H}_2\text{O}}^2}{p_{\text{H}_2}^2 p_{\text{O}_2}} = \frac{(1 - 2x)^2 (2 + x + y)}{(1 + 2x)^2 x} \quad [3]$$

and for the equilibrium given by Eq. [2]

$$7.87 \times 10^5 = \frac{p_{\text{H}_2}}{p_{\text{H}}^2} = \frac{(1 + 2x - y)(2 + x + y)}{(2y)^2} \quad [4]$$

Simultaneous solution of Eqs. [3] and [4] gives

$$x = 1.424 \times 10^{-7} \text{ and } y = 7.969 \times 10^{-4}$$

Thus, in the equilibrated gas mixture,

$$p_{\text{O}_2} = \frac{x}{2 + x + y} = 7.12 \times 10^{-8} \text{ atm and}$$

$$p_{\text{H}} = \frac{2y}{2 + x + y} = 7.97 \times 10^{-4} \text{ atm}^{(1)}$$

Thus, although inclusion of the consideration of the dissociation of molecular hydrogen provides a more rigorous treatment of the equilibria in a H₂-H₂O gas mixture, the small extent of dissociation has an insignificant influence on the calculated partial pressure of oxygen and, hence, on the reducing power of the mixture. Complete rigor would require that the dissociation of molecular oxygen be considered, in which case the equilibrium system would contain five species and would involve three independent equilibria.

The errors in Robino's analysis involve consideration of a single reaction equilibrium in a two-component system containing four species, given by his Eq. [5], and the assumption that the fraction of hydrogen occurring as atomic hydrogen, defined by his Eq. [9], is an independent variable. The mole fraction of atomic hydrogen in the gas is determined by temperature, total pressure, and the initial ratio of H₂ to H₂O in the gas mixture.

REFERENCES

1. C.V. Robino: *Metall. Mater. Trans. B*, 1996, vol. 27B, pp. 65-69.

Author's Reply

C.V. ROBINO

The author would like to thank Professor Gaskell for his thoughtful discussion of the referenced article. In his dis-

*C.V. ROBINO: *Metall. Mater. Trans. B*, 1996, vol. 27B, pp. 65-69.
D.R. GASKELL, Professor, is with the School of Materials Engineering, Purdue University, West Lafayette, IN 47907.
Discussion submitted March 14, 1996.